Nanometer-Scale Chemistry of a Calcite Biomineralization Template: Implications for Skeletal Composition and Nucleation

Oscar Branson[a,1,2,3], Elisa A. Bonnin[b], Daniel E. Perea[c], Howard J. Spero[a,3], Zihua Zhu[c], Maria Winters[c], Bärbel Hönisch[d], Ann D. Russell[a], Jennifer S. Fehrenbacher[a,e], and Alexander C. Gagnon[b,3]

[a]Department of Earth and Planetary Sciences, University of California, Davis, CA 95616; [b]School of Oceanography, University of Washington, Seattle, WA 98195; [c]Environmental Molecular Science Laboratory, Pacific Northwest National Laboratory, Richland, WA 99352; [d]Department of Earth and Environmental Sciences, Lamont-Doherty Earth Observatory of Columbia University, Palisades, NY 10964; and [e]College of Earth, Ocean, and Atmospheric Sciences, Oregon State University, Corvallis, OR 97331

Edited by Patricia M. Dove, Virginia Tech, Blacksburg, VA, and approved September 23, 2016 (received for review November 19, 2015)

Plankton, corals, and other organisms produce calcium carbonate skeletons that are integral to their survival, form a key component of the global carbon cycle, and record an archive of past oceanographic conditions in their geochemistry. A key aspect of the formation of these biominerals is the interaction between organic templating structures and mineral precipitation processes. Laboratory-based studies have shown that these atomic-scale processes can profoundly influence the architecture and composition of minerals, but their importance in calcifying organisms is poorly understood because it is difficult to measure the chemistry of in vivo biomineral interfaces at spatially relevant scales. Understanding the role of templates in biomineral nucleation, and their importance in skeletal geochemistry requires an integrated, multiscale approach, which can place atom-scale observations of organic-mineral interfaces within a broader structural and geochemical context. Here we map the chemistry of an embedded organic template structure within a carbonate skeleton of the foraminifera *Orbulina universa* using both atom probe tomography (APT), a 3D chemical imaging technique with Ångström-level spatial resolution, and time-of-flight secondary ionization mass spectrometry (ToF-SIMS), a 2D chemical imaging technique with submicron resolution. We quantitatively link these observations, revealing that the organic template in *O. universa* is uniquely enriched in both Na and Mg, and contributes to intraskeletal chemical heterogeneity. Our APT analyses reveal the cation composition of the organic surface, offering evidence to suggest that cations other than Ca^{2+}, previously considered passive spectator ions in biomineral templating, may be important in defining the energetics of carbonate nucleation on organic templates.

biomineralization | templating | foraminifera | geochemistry | paleoceanography

The formation of calcium carbonate biomineral skeletons is integral to the survival of diverse groups of marine organisms (1) and is a major component of the global carbon cycle (2). Ancient $CaCO_3$ skeletons preserve a chemical archive of the oceanographic conditions they were formed in, and provide one of our most comprehensive geochemical records of past climate (3). Despite the role that biomineralization plays in evolution, global chemical cycling, and our understanding of past climate, we lack a complete mechanistic understanding of biomineral growth that can predict how it responds to environmental change, and affects shell geochemistry.

Calcification is particularly complex because it is affected by both environmental and biological factors. During biomineralization, organisms control the flow of ions, manipulate aqueous speciation, and use organic–mineral interactions to modulate the morphology, composition, and growth rate of skeletal minerals (4). Of these processes, the role of organic–mineral interactions is the least understood, and has the most potential to revise our understanding of the balance between environmental and biological control during skeletal growth. The formation of many carbonate biominerals begins around organic templating structures (5), where atomic-scale interactions between organic surfaces and mineral growth processes define the gross architecture of the biomineral (4). At a mechanistic level, these organic–mineral interactions facilitate heterogeneous nucleation processes, and allow an organism to overcome chemical and physical barriers to crystal nucleation and growth (4, 5). Organic–mineral interactions may also influence the composition of biominerals (6, 7). Many $CaCO_3$ biominerals exhibit complex, systematic intraskeletal chemical variability (e.g., refs. 7–10), which cannot be explained by external environmental factors. Given the use of biomineral geochemistry as a tool to explore past climate change, it is important to understand the mechanisms controlling these patterns. This is particularly relevant today, as technological advances have improved the spatial resolution and sensitivity of geochemical analyses to the point where intraskeletal chemical variability can directly influence geochemical paleoclimate records (8, 11). It is critical to know how organic components affect skeletal growth and composition, and whether these organic-associated features can be distinguished from environmental signals.

Laboratory-grown mineral templating experiments show that the charge and structure of organic additives can affect crystal morphology (4, 12), polymorph (13), composition (14), orientation and nucleation rate (15). In vitro studies have also revealed that

Significance

Many marine organisms build complex $CaCO_3$ shells, which record an archive of past climate in their trace chemistry. Organic–mineral interactions are a crucial, poorly understood aspect of shell formation, which may alter shell composition and bias climate records. We map the chemistry of an organic template preserved within a type of shell that is widely used in studies of past climate. We find that the organic template embedded within this shell is enriched in Na and Mg, and can locally influence shell composition. Atom-scale maps of template chemistry offer a detailed view of the chemical interactions at an organic mineral template, and suggest that elements other than Ca^{2+} may be important in defining the energetics of $CaCO_3$ nucleation during biomineralization.

Author contributions: O.B., D.E.P., H.J.S., and A.C.G. designed research; O.B., E.A.B., D.E.P., Z.Z., M.W., and A.C.G. performed research; D.E.P. and Z.Z. contributed new analytic tools; O.B., E.A.B., D.E.P., Z.Z., M.W., and A.C.G. analyzed data; B.H., A.D.R., and J.S.F. were essential in culturing foraminiferal specimens for the study; and O.B., H.J.S., and A.C.G. wrote the paper.

The authors declare no conflict of interest.

This article is a PNAS Direct Submission.

[1]O.B. and A.C.G. contributed equally to this work.

[2]Present Address: Research School of Earth Sciences, Australian National University, Acton ACT 2601, Australia.

[3]To whom correspondence may be addressed. Email: oscarbranson@gmail.com, hjspero@ucdavis.edu, or gagnon@uw.edu.

This article contains supporting information online at www.pnas.org/lookup/suppl/doi:10.1073/pnas.1522864113/-/DCSupplemental.

Ca-specific recruitment to the template surface is an important primary step in carbonate nucleation (16), and it is commonly proposed that similar interactions are also crucial within mineralizing organisms (5). However, the importance of the interactions observed during in vitro experiments to biomineralization is poorly understood, because the chemistry of in situ organic templating surfaces in calcifying organisms is extremely hard to observe at spatially relevant scales. Observations of the atomic-scale chemistry of organic–mineral interfaces could tell us which chemical species and interactions are most crucial for nucleation within biominerals, and help build a detailed mechanistic understanding of biomineralization. However, to fully evaluate the role of organics in nucleation and shell geochemistry, we need multiscale analyses that can place atom-scale measurements of template chemistry in the context of skeletal-scale compositional patterns. If we can link these scales, we can be confident that our atom-scale observations capture the chemical patterns of templating processes, and test whether these organic components exert a measurable effect on shell geochemistry.

The planktic foraminifera *Orbulina universa* (Fig. 1) provides an ideal system for studying mineral-associated organics. Foraminifera are a cosmopolitan group of marine protozoans with a fossil record that extends back to the earliest Cambrian period (17), offering one of the most comprehensive geochemical archives of past climate and ocean chemistry (3). *O. universa* has been extensively used as a model organism for studying foraminiferal biomineralization and geochemistry (e.g., ref. 11). The $CaCO_3$ "test" (shell) contains a single, embedded organic structure known as the primary organic sheet (POS*; Fig. 1 *B* and *C*; 18, 19), which is produced during the initial stage of skeletal formation, and is composed of polysaccharides and acidic amino acids (20, 21). Little is known about the specifics of POS structure and formation, but studies of analogous structures in other organisms (22, 23) suggest that the polysaccharide component provides structural integrity to the organic template, and the acidic amino acids guide calcite nucleation (24). The fluids surrounding the POS are thought to originate from seawater, and are modified by unknown mechanisms before calcification (6, 7, 19). In *O. universa*, nucleation and mineral growth occurs on both sides of the POS, encasing the organic templating structure within the biomineral (18). This embedded POS can be located within the test (shell, Fig. 1), and offers an ideal target for a multiscale investigation of organic template chemistry in *O. universa*.

We use atom probe tomography (APT, ref. 25) to measure the atom-scale chemistry of the interface between the POS and the carbonate mineral skeleton in *O. universa*, and provide a compositional map of an organic template surface in a carbonate biomineral. This technique precisely determines the 3D position and identity of individual ions evaporated from a solid sample to within ~2 Å [~0.2 nm (25)], using a combination of field ion microscopy and time-of-flight mass spectrometry. Recent developments have allowed the application of APT to a range of natural materials (26–29) but carbonate minerals, which are by far the most abundant and diverse biomineral group produced in the plant and animal kingdoms, remain challenging targets for APT analysis. The structural heterogeneity, high evaporation field, and low thermal and electrical conductivity of carbonate biominerals make them a difficult material for analysis by routine APT techniques. We have optimized sample preparation and APT analysis parameters (*SI Appendix*, sections 3.1 and 3.2), and obtained APT data from a biomineral $CaCO_3$–organic interface. These analyses are given context by 2D chemical maps of the entire shell wall, collected using time-of-flight secondary ionization mass spectrometry (ToF-SIMS). ToF-SIMS is similar to the more established nano-SIMS technique used in previous studies (9, 30), but uses a time-of-flight mass separation device instead of a magnet to simultaneously measure a wide range of masses.

*The POS has previously been called the "primary organic membrane", but because it is not a membrane in the biological sense (i.e., a phospholipid bilayer), we adopt the "POS" nomenclature advocated by de Nooijer et al. (19).

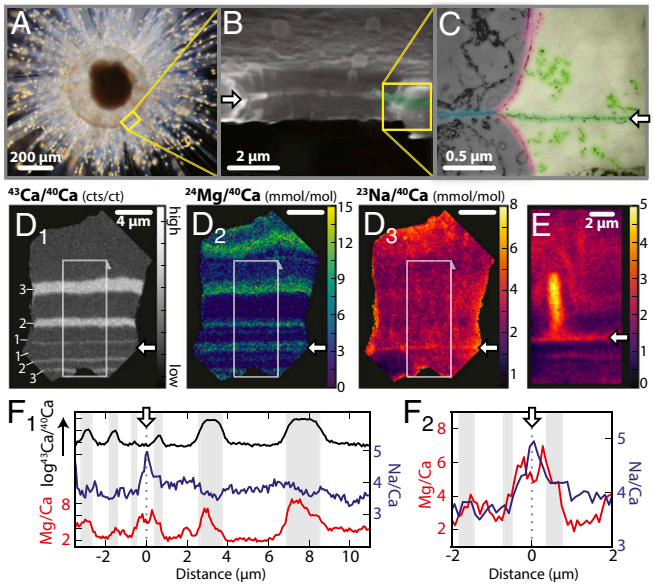

Fig. 1. The spherical shell of *O. universa* is constructed around a POS and is chemically heterogeneous. (*A*) Light micrograph of *O. universa* with a newly calcified spherical chamber surrounded by calcite spines and cellular material. Bright points on the spines are symbiotic dinoflagellates. (*B*) SEM of a 1-d-old calcite sphere, broken to expose a wall cross-section and shell pore. The white arrow identifies the embedded POS, which is visible as a raised ridge in the cross-section. Calcite precipitation occurs on both sides of the POS. (*C*) TEM of the cross-section of an agar-mounted decalcified shell wall (paler, *Right*) and pore (darker, *Left*). The POS (green horizontal layer, white arrow) is visible within the decalcified shell. The pore has an organic lining (red), and "pore plate" (blue) contiguous with the POS. For a detailed discussion of these features, see ref. 18. The POS appears to be a complex, branched structure rather than a continuous sheet, with numerous electron-dense regions of similar structure to the POS extending ~500 nm either side of the POS (light green). SEM and TEM images were generated following methods in ref. 18. (*D* and *E*) ToF-SIMS $^{43}Ca/^{40}Ca$, $^{24}Mg/^{40}Ca$, and $^{23}Na/^{40}Ca$ maps of cross-sections through a mature, 4-d-old shell wall. This foraminifera was moved between ^{43}Ca enriched seawater at night, and "natural" seawater during the day, resulting in three ^{43}Ca enriched bands on each side of the POS. The position of the POS (white arrows) is bracketed by these symmetric ^{43}Ca "labels" (numbered in D_1; *SI Appendix*, section 2.4), which identify the origin of calcification and constrain the location of the POS (white arrow). The region associated with the POS has elevated Na and Mg. *E* captures the base of a Na-rich calcite spine within the shell wall of a different specimen. The spines originate at the POS (18), further identifying the Na-rich band in D_3 as associated with the POS. Profiles in F_1 are extracted from white boxes in *D*, and enlargements in F_2 highlight the coincident Mg/Ca and Na/Ca maxima that are uniquely present at the POS. The double Mg maxima either side of the Na maximum in this specimen is present in ~33% of specimens, and is caused by the POS being between two, close high-Mg bands. A more typical signal can be seen in *SI Appendix*, section 2.4.

Results and Discussion

ToF-SIMS: Submicrometer 2D Maps. ToF-SIMS maps of skeletal chemistry across a wide range of elements (up to 72 amu) were collected using a 312-nm Bi^{+} analysis beam with a step size of 78.1 nm. This allows the detection of intraskeletal features at a minimum resolvable distance of 370 nm, beyond the resolution limits of previous techniques (e.g., ref. 31). Among the wide range of elements analyzed by ToF-SIMS, Mg and Na alone were found to exhibit systematic heterogeneity perpendicular to the growth axis of the shell (Fig. 1*D*). Magnesium variability confirms previous observations of intratest Mg heterogeneity in *O. universa* (8, 11, 31). Sodium variability is of lower magnitude, except for a single fine band that is uniquely enriched in both Na and Mg (Fig. 1 *D* and *F*). This feature is present in all specimens analyzed, occurring only once in each specimen. Within this band Na and Mg are elevated by 49 ± 20% and 147 ± 85% (n = 18),

respectively, relative to the adjacent mineral, with a full-width-at-half-peak-maxima (FWHM) of 673 ± 272 nm (n = 18). In most specimens, this band contains the highest concentration of Na in the whole skeleton, whereas the Mg concentration is within the range of other skeletal variations. Other elements known to exhibit systematic banding in *O. universa* (e.g., S:7, 9; B:10) were not detected by ToF-SIMS.

The position of the POS in ToF-SIMS maps is constrained by culturing foraminifera with a ^{43}Ca pulse-chase label, which produces symmetric layers of ^{43}Ca-enriched calcite on either side of the POS (Fig. 1D_1 and *SI Appendix*, section 2.4). The coincident Mg and Na enriched band is consistently located within the innermost ^{43}Ca bands, associated with the location of the POS (Fig. 1 *D* and *F*). Additional evidence that this feature is associated with the POS is provided by ToF-SIMS maps which contain the base of a "spine" (Fig. 1*E*), a calcite structure which is known to originate at the POS and protrude through the shell wall [Fig. 1*A* (18)]. These maps reveal that the spines are significantly enriched in Na, and terminate at the Na and Mg enriched band within the skeleton.

Sodium variability away from the POS is of lower amplitude, broader, and not clearly associated with sharp Mg maxima. Because these variations are unlikely to be associated with organic components (32), further discussion is outside the scope of this study and will be described in detail elsewhere. The ability to identify the location of the POS by the presence of simultaneous Mg and Na maxima using ToF-SIMS offers a way to map the location of organic components in foraminifera, and allows us to specifically target this important structure in our APT analyses.

APT: Subnanometer 3D Maps. Using APT, we map the 3D chemistry of the interface between an embedded organic structure and the adjacent calcite within a single foraminiferal specimen. Within our APT data volume, calcite is identified by its high Ca content relative to the organic layer, which was low in Ca but rich in C and H (Figs. 2 and 3). The organic layer is further distinguished from calcite by the types of C-containing ions emitted from each material during analysis (*SI Appendix*, section 3.3.4). The organic material yielded significantly fewer ions than calcite. This is expected, given the dependence of field evaporation on the bond strength of atoms (33), and prevalence of strong covalent bonds within organic material. However, it is likely that organic-hosted cations would be ionically bound and ionize relatively easily, making cation measurements from the organic more accurate than nonmetals.

In the APT reconstruction (Fig. 2), the calcite and organic regions are separated by a continuous, broadly planar interface that is defined by an abrupt change in Ca, C, and H over ∼2 nm. This interface is operationally identified by a 50% Ca isoconcentration surface (Fig. 2*A*), which is slightly curved and exhibits some nonsystematic roughness, manifest as surface undulations with a 5–10-nm period, and 1–2-nm amplitude. Compositional profiles across this boundary (proxygrams, Fig. 3) reveal an abrupt increase in Na and Mg concentration in the organic layer, compared with the calcite. Magnesium is variable throughout the organic layer with maxima ∼3 and ∼6 nm into the organic material. Sodium has a distinct maximum on the organic side of the interface, and a secondary maximum at ∼5 nm into the organic (Fig. 3*B*). The variability of Na and Mg within the organic layer may be taken to suggest an ∼5-nm periodicity, which could relate to aspects of the formation or structure of the organic layer, which are poorly constrained. At its surface maximum Na/Ca reaches a ratio of ∼0.6 counts/count, which corresponds to more than one Na for every two Ca detected at the surface of the organic layer. The lower evaporation rate of the organic layer can lead to the evolution of local topography during data collection, and deflect interfacial ions away from the organic toward the calcite (34). The compositional patterns on the organic side of the interface may therefore be conservatively constrained to the surface of the organic material, whereas ions on the calcite side may originate from either calcite or organic parts of the sample. Together with the ∼0.2-nm resolution of APT, this allows us to conservatively constrain the location of this Na maximum to the outer 1–2 nm of the organic layer, rather than at the interfacial boundary, or within the layer of calcite immediately adjacent to the organic surface.

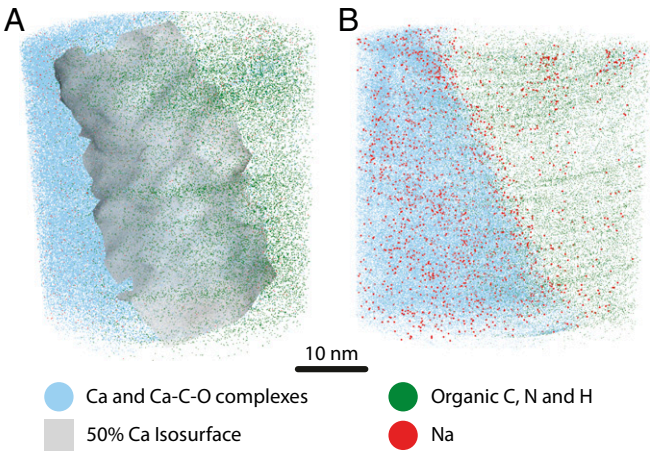

Fig. 2. Three-dimensional APT reconstruction of a planar organic-mineral templating surface within foraminiferal calcite. (*A*) The APT reconstruction captures the interface between calcite (Ca-rich) and an organic (Ca-poor) region. The structure of this predominantly planar interface is highlighted by a 50% Ca-concentration isosurface. (*B*) When viewed in plane with the interface, Na appears elevated at the interface. The symbols for Na have been enlarged 2× for emphasis. Note that whereas Na appears more abundant on the calcite side of the interface, this reflects the higher ionic yield from calcite than the organic layer, and by atomic fraction Na is more abundant in the organic layer, as highlighted in Fig 3.

The calcite layer is compositionally homogeneous at the scale of APT analyses, with 4.6 ± 0.7 counts/kcounts Mg/Ca and 7.6 ± 0.1 counts/kcounts Na/Ca, and no interface-specific compositional patterns. To investigate the influence of instrumental bias on APT-derived compositions, we compared the composition of calcite measured by both ToF-SIMS and APT in the same specimen. In ToF-SIMS, calcite adjacent to the POS contains ∼6.6 mmol/mol Mg/Ca and ∼3.6 mmol/mol Na/Ca (Fig. 1), suggesting that the uncalibrated APT analyses underestimate Mg/Ca by a factor of ∼0.7 and overestimate Na/Ca by a factor of ∼2 in calcite. Whereas this provides a rough estimate of instrumental bias, it is not possible to use this comparison with directly calibrate APT data, because ToF-SIMS analyses are unable to resolve calcite chemistry on the scale of APT analyses, and templating interactions may influence the chemistry of the initial calcite layer. The major element composition of the organic layer is uniform, with a measured stoichiometry of approximately $C_4O_3H_2$. However, the low yield of nonmetal elements in both the calcite and the organic layers likely biases this measurement.

Connecting Spatial Scales. The organic material observed by APT is elevated in both Na and Mg, and the only region in ToF-SIMS data consistently elevated in both Na and Mg is at the POS. This qualitative correspondence suggests that the organic layer observed in APT data could be the POS, but differences in the scale of the analyses preclude a direct quantitative comparison. Given the possible occurrence of non-POS organics within foraminifera (35), we test whether the organic layer captured by APT is compositionally consistent with the POS-associated chemical signal observed by ToF-SIMS using a quantitative model.

Because APT and ToF-SIMS integrate over different spatial scales, the magnitude of both Mg and Na signals will be different between the techniques, but the relative enrichment of Mg and Na within one method must match the other. To test this, we calculate the simultaneous Na and Mg enrichment that would be observed by ToF-SIMS when measuring an organic layer embedded in a calcite substrate, based on APT-measured compositions of the two materials. This model tests the hypothesis that the POS-associated

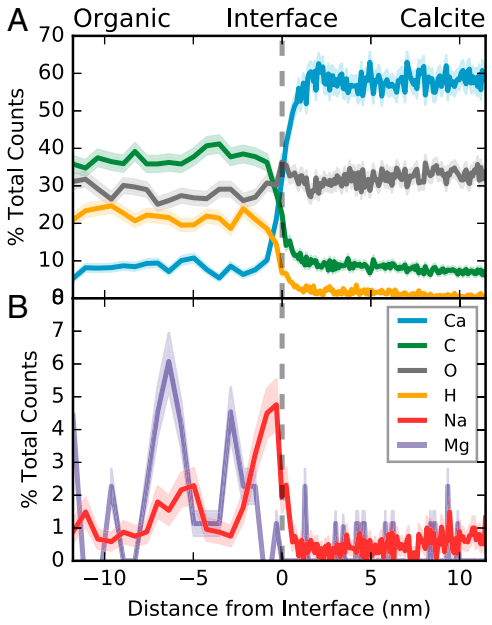

Fig. 3. Compositional profiles through the APT reconstruction reveal Na enrichment in the organic surface. (*A*) Chemical profiles ("proxygrams") across the biomineral interface in Fig. 2 quantify sharp changes in major elements across an ∼2-nm interface, defining the transition between the calcite and organic layers (dashed line). Profiles are presented as percent of collected ions, with profile bins defined using a constant number of ions per bin. Shaded error envelope calculated based on counting statistics. (*B*) Both Na and Mg are elevated in the organic material relative to the calcite. This enrichment is not centered on the interface, but instead occurs within the first few nanometers on the organic side of the interface.

signal observed in ToF-SIMS is derived from a material of similar composition to the ∼10-nm organic layer measured by APT. The inputs to our model are the volume-normalized APT counts of Ca, Na, and Mg from each material, the ToF-SIMS beam size (312 nm), and the width of the simulated POS. The POS width is unconstrained, and is tuned to match the absolute magnitude of Na and Mg enrichment observed in ToF-SIMS. Whereas POS width changes the absolute amplitude of the Na and Mg enrichment, it does not change their relative magnitude. We may therefore accept our hypothesis if our APT-based model can simultaneously predict both the Mg and Na enrichment observed in ToF-SIMS using only a single POS width.

Because the APT ion ratios are uncalibrated, we model the relative magnitude of the organic-driven increase above the adjacent background calcite. This approach allows for variable ionization efficiency between Ca, Mg, and Na in APT. We assume that this bias is similar for the three metals between organic and calcite layers. Within these constraints, our model accurately predicts both the Na and Mg enrichment observed by ToF-SIMS (Fig. 4 and *SI Appendix*, section 4), demonstrating that the POS-associated signal observed in ToF-SIMS is consistent with an organic material of the same average composition as the organic layer measured by APT. This provides an important test of the consistency between APT and ToF-SIMS data, and connecting these atom- and submicrometer-scale observations constitutes a significant step forward in correlative chemical microscopy. The strong correspondence between these scales demonstrates that the Mg and Na maxima in the ToF-SIMS data are likely caused by the same organic material measured by APT. This reveals that the POS can contribute to intraskeletal chemical patterns in foraminifera.

Within our model, the absolute amplitude of the predicted signal depends upon the thickness of the POS. This offers an estimate of POS width that is independent of the relative Na and Mg enrichment used to evaluate our hypothesis. The amplitudes of the ToF-SIMS Na and Mg maxima are consistent with an ∼130-nm-thick POS, in agreement with previous POS width estimates [∼100 nm, Fig. 1 (18)]. In contrast, the width of the POS-associated ToF-SIMS signal is more consistent with a POS thickness of ∼700 nm. Oblique sample sectioning could broaden the linear features in ToF-SIMS analysis, but is insufficient to explain the approximately sixfold difference between both previous transmission electron micrograph (TEM) analyses and ToF-SIMS peak widths (*SI Appendix*, section 1.2). This discrepancy may be accommodated if the POS is not a single laminar organic structure, as previously proposed (18, 19), but a dispersed organic framework that is concentrated around the origin of calcification. Our suggestion of a more complex POS geometry is supported by careful examination of *O. universa* TEM and SEM images [Fig. 1*C* (18)]. Whereas sample preparation procedures may alter or displace the delicate structures in these images, they show that the POS is branched and multifaceted, implying a larger effective width than a single, laminar structure. In line with this observation, we also observed two smaller organic structures in APT samples extracted away from the POS (*SI Appendix*, section 3.4).

Organics and Foraminiferal Geochemistry. Systematic variations in the intrashell concentrations of Mg, S, and B are widely recognized in *O. universa* and other foraminifera (Mg:8, 31, 32; S:7, 9;

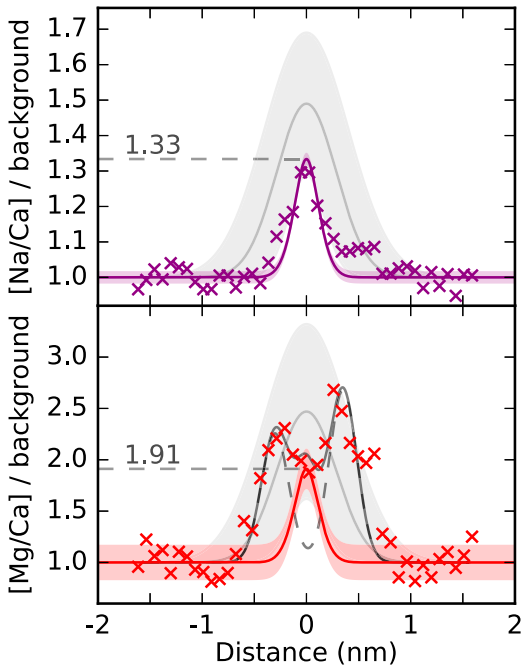

Fig. 4. Observed POS-specific Na and Mg maxima in ToF-SIMS can be explained by APT measurements, suggesting that both techniques are imaging the same structure. ToF-SIMS and APT cannot be directly compared because of differences in spatial scale. Instead, the relative magnitude of the POS Na and Mg enrichment measured by ToF-SIMS (crosses) are compared with APT measurements of POS composition (solid lines) in the same specimen using a quantitative model. The shaded gray envelopes show the mean and SD of the POS-associated signal in 18 other ToF-SIMS specimens, and highlight a degree of variability in Na and Mg enrichment between individuals. Modeled intensities are based on APT measured compositions, a beam width of 312 nm, and a POS thickness of 130 nm. The double Mg peaks bracketing the POS can be explained by two Gaussians with 312-nm FWHM (dashed peaks), consistent with two narrow bands of higher-Mg calcite ∼300 nm either side of the POS. At this distance, the contribution of these peaks to the POS location is negligible. The combination of these Gaussian peaks and the modeled POS signal (solid black line) describe the POS-associated Mg maxima in this specimen (*SI Appendix*, section 4.5).

B:10), but the mechanisms driving this variability are poorly constrained. Hypotheses range from physiological processes altering the chemistry of calcification (11), to the inclusion of organic components within the structure (6, 7), with many models in between. Our atom-scale characterization of POS composition "scales up" to quantitatively explain the POS-associated compositional patterns observed in a 2D map of the same specimen, demonstrating that the POS can drive localized enrichments in both Na and Mg in *O. universa*. However, because there is only one POS in *O. universa* (18), other processes must account for the intrashell chemical heterogeneity seen elsewhere in the shell, like Mg/Ca "banding." This is consistent with X-ray analyses of Mg enrichment away from the POS in *O. universa*, which reveal that non-POS Mg is not hosted in organic structures (32). Thus, the presence of organic components can explain an important aspect of, but not all, intrashell Mg and Na heterogeneity in *O. universa*.

The correspondence between our APT observations and ToF-SIMS data demonstrates that the POS can contribute to intraskeletal chemical heterogeneity and may impact paleo reconstructions based on highly resolved analytical techniques. This raises the important question of whether organic components may influence the bulk geochemistry of *O. universa*, and affect paleoceanographic records. The similarity between ToF-SIMS observations of POS composition in 19 *O. universa* specimens offers an important level of confidence that observations from our single APT specimen may be more broadly applicable to *O. universa* as a whole, and allow us to evaluate the importance of organics to the overall geochemistry of *O. universa*.

The Mg/Ca of foraminifera is a well-established proxy for past ocean temperature (36), and Na/Ca is being considered as a proxy for ocean salinity (37). We calculate the contribution of the POS to bulk Mg/Ca and Na/Ca in *O. universa* based on our APT measurements, by extending the APT-based model applied to predict our ToF-SIMS observations to the bulk scale (*SI Appendix*, section 4.6). The contribution of the POS decreases logarithmically as shell thickness increases, and will add >0.5 °C to a Mg/Ca-derived temperature estimate at a shell thickness below ∼4.6 μm, and increase a salinity estimate by >1 practical salinity unit below ∼2.5 μm. Because thin-shelled foraminifera are rarely preserved in marine sediments, the POS is unlikely to be important in paleoceanographic applications of *O. universa*. However, the POS should be carefully considered when creating paleoproxy calibrations from cultured foraminifera, where thin-shelled specimens may be included in analysis. Furthermore, the majority of paleoceanographic analyses measure the chemistry of multichambered foraminifera, which may contain multiple organic layers (7, 19). If these organic layers are all enriched in Mg and Na, they may contribute significantly to bulk geochemistry. Quantifying the magnitude of these possible effects requires further investigation and characterization of the composition and frequency of organic layers within multichambered foraminifera. To this end, the POS-associated Na and Mg signal identified in this study may offer a promising new way to map the number and location of organic layers within the skeletons of more complex, multichambered foraminifera.

Pattern to Mechanism: Insights into Nucleation Processes. Given the presence of a POS-associated Na and Mg maximum in all 19 *O. universa* specimens analyzed, and the quantitative correspondence between our APT and ToF-SIMS datasets, it is likely that our APT measurement is a representative example of POS chemistry in *O. universa*. The distinctive atom-scale surface chemistry patterns may therefore provide new insights into the factors influencing template-directed calcite nucleation during biomineralization. The compositional patterns at the POS surface may be the result of the active or passive interaction of cations with a templating surface, increased trace element uptake into the initial calcite layer by template-induced lattice strain, or the exclusion of non-$CaCO_3$ ions from a crystal nucleating on the surface. The position of the Na maximum ∼1 nm on the organic side of the 50% Ca isosurface, before any appreciable increase in Ca concentration, conservatively constrains the location of the Na maximum to within the organic surface; it is neither at the interphase boundary between the template and mineral nor within the initial mineral layer. This suggests that the Na maximum is either the result of solute ions interacting with the template surface, or the exclusion of ions from crystal nuclei that are taken up into the organic surface. In either case, non-Ca^{2+} ions accumulate at the POS surface before or during heterogeneous nucleation.

The compositional patterns we observe at the surface of the POS may be altered up to the point at which the organic template is "buried" by crystalline carbonate, and can no longer exchange ions with solution. The POS surface Na maximum is enriched in both Ca^{2+} and Mg^{2+}, relative to the abundance of the cations in seawater (78% Ca, 18% Na, 4% Mg, or 39:9:2 vs. 1:50:5 in seawater; Fig. 3). This supports the preferential accumulation of Ca^{2+} at the template surface, as commonly suggested by analogous synthetic studies (5), but also suggests the simultaneous adsorption of non-Ca^{2+} ions. Because the chemistry of the calcification environment is unknown, we cannot distinguish whether these ions accumulate "passively" in proportion to their abundance in solution, or "actively" through ion-specific interactions with the organic surface. Regardless of the driving mechanism, the composition of the POS surface will influence the interaction between the biological template and crystal nuclei.

For nucleation to occur, ions must overcome an energetic barrier to reorganize into a new solid phase. One of the main factors controlling the magnitude of this barrier, and thus the likelihood of nucleation, are the interfacial energies between template, solution, and mineral (38). This is true for both ordered and amorphous calcium carbonate phases (39). Changes in the organic surface charge (38, 40), degree of structural similarity to the crystal (41), and ordering of water molecules adjacent to the surface (42) can each alter the interfacial energy of the template, and change the dynamics of nucleation. The presence of Na and Mg at the organic template surface can influence each of the surface properties that contribute to interfacial energy.

The ability of specific ions to stabilize or disrupt organic–water interfaces by modifying surface hydration or direct ion-pairing interactions is described by the Hofmeister series (42–44). Broadly, an organic–water interface is stabilized by weakly positive or strongly negative ions, and destabilized by strongly positive or weakly negative ions. The major seawater cations are strongly charged, and will tend to exert a destabilizing (chaotropic) influence, increasing the organic–water interfacial energy. The strength of these effects is ion specific, and sensitive to organic surface structure and solute composition (43, 45, 46).

Sodium and magnesium are major components of POS surface chemistry, making up 18% and 4% of the detectable surface "cation load." Given the differences in size and charge density between these ions, each may have a distinct effect on the surface properties of the mineral template, alter the barriers to nucleation, and affect the energetics of biomineralization as a whole (38). Because of its relatively strong chaotropic influence, it is likely that Mg^{2+} will be a particularly potent modifier of surface properties, although the greater abundance of Na^{+} at the surface may make its overall contribution more significant.

Studies have considered the effect of overall ionic strength on in vitro template-facilitated mineral nucleation (38), but the effects of specific solute ions on nucleation energetics proposed here have yet to be explored. Our study highlights the need for inorganic nucleation experiments to investigate the effects of non-Ca^{2+} ions, which are currently thought to be "spectator ions" in nucleation, on the energetics of template-directed nucleation. In particular, determining the magnitude and direction of the proposed ion-specific effects is essential to evaluate their importance to biomineralization. If the abundance of Mg^{2+} and Na^{+} at the POS surface is related to their concentration in seawater, the chemical patterns at the POS surface offer an intriguing connection between changes in seawater composition through time and the energetics of biomineralization.

Methods

Foraminifera Culturing. Specimens of the foraminifera *O. universa* were hand-collected (47), and individual foraminifera were cultured following standard methods (48) at 21 °C on a 12-h/12-h day–night light cycle in ambient seawater of known composition (*SI Appendix*, section 1.1).

ToF-SIMS Data Collection. The terminal spherical calcite chambers of *O. universa*, which grew completely in the laboratory, were chemically cleaned of surface-associated organic material using a hot NaOH H_2O_2 solution, mounted in Araldite epoxy resin and polished to expose the test cross-section, and gold coated for analysis (*SI Appendix*, section 1.2). Polished specimens were analyzed in a TOF.SIMS5 (IONTOF GmbH, Germany) ToF-SIMS with a 25 keV Bi^+ ion beam with a pulsed beam current of 0.66 pA, and a measured beam width of 312 nm (FWHM). Data were collected between 0 and 78 amu, and specific peaks corresponding to $^{23}Na^+$, $^{40}Ca^+$, $^{43}Ca^+$, and $^{24}Mg^+$ were identified. Resulting maps and profiles are the sum of 1,600 analyses collected over 2 h for each location (*SI Appendix*, section 2.1).

APT Data Collection. APT specimens were extracted from the polished foraminiferal test and sharpened through focused ion beam lift-out techniques (49) using a Helios NanoLab 600 (*SI Appendix*, section 1.3). Specimens were extracted from within ~1 μm of the location of the POS, as determined by the position of ^{43}Ca-enriched bands (Fig. 1). APT data were collected using a Cameca LEAP 4000X-HR instrument at 44 K with a 50-pJ 355-nm laser pulsed at 160–200 Hz. Data were reconstructed with Cameca's Integrated Visualization and Analysis Software, using measurements of pre- and post-analysis SEM images of the sample to constrain the volume.

APT Data Processing. Ion identities were assigned to Da ranges based on sample composition (*SI Appendix*, section 3.3.1). The biomineral interface was defined as the 50% Ca concentration isosurface (*SI Appendix*, section 3.3.4). Proxygram profiles for every spectral peak and associated background regions were taken normal to the interface, and imported into Python for analysis (*SI Appendix*, section 3.3.5). After background subtraction, proxygram profiles were rebinned to maintain a constant total ion count in each bin, making counting statistics comparable. Na counts were calculated by subtracting predicted $^{46}Ca^{2+}$ from the 23-Da peak, calculated based on the natural abundance of Ca isotopes and the counts of $^{40}Ca^{2+}$. Mg counts were calculated based on the $^{26}Mg^+$ and $^{25}Mg^{2+}$ peaks (*SI Appendix*, section 3.3.2). Atomic compositions were calculated from the background-corrected counts, based on the composition assigned to each peak. Further detail on sample preparation, analysis, and processing can be found in the *SI Appendix*.

ACKNOWLEDGMENTS. We thank Adam Wallace for insightful discussions. This research was supported in part by US National Science Foundation Awards 1420689 (to A.C.G.), 1061676 (to H.J.S.), 1261519 (to A.D.R. and J.S.F.), and 1232987 (to B.H.). APT and ToF-SIMS analysis was supported through User Proposal 48564 to A.C.G., part of a Special Science Call at the Environmental Molecular Sciences Laboratory, a Department of Energy Office of Science User Facility sponsored by the Office of Biological and Environmental Research and located at Pacific Northwest National Laboratory.

1. Knoll A (2003) Biomineralization and evolutionary history. *Rev Mineral Geochem* 54(1):329–356.
2. Elderfield H (2002) Climate change. Carbonate mysteries. *Science* 296(5573):1618–1621.
3. Katz ME, Cramer BS, Franzese A, Hönisch B (2010) Traditional and emerging geochemical proxies in foraminifera. *J Foraminiferal Res* 40(2):165–192.
4. de Yoreo JJ, Wierzbicki A, Dove PM (2007) New insights into mechanisms of biomolecular control on growth of inorganic crystals. *CrystEngComm* 9(12):1144–1152.
5. Gilbert PUPA, Abrecht M, Frazer BH (2005) The organic-mineral interface in biominerals. *Rev Mineral Geochem* 59(1):157–185.
6. Bentov S, Erez J (2006) Impact of biomineralization processes on the Mg content of foraminiferal shells: A biological perspective. *Geochem Geophys Geosyst* 7(1):Q01P08.
7. Erez J (2003) The source of ions for biomineralization in foraminifera and their implications for paleoceanographic proxies. *Rev Mineral Geochem* 54:115–149.
8. Eggins S, de Deckker P, Marshall J (2003) Mg/Ca variation in planktonic foraminifera tests: Implications for reconstructing palaeo-seawater temperature and habitat migration. *Earth Planet Sci Lett* 212(3):291–306.
9. Paris G, Fehrenbacher JS, Sessions AL, Spero HJ, Adkins JF (2014) Experimental determination of carbonate-associated sulfate $\delta^{34}S$ in planktonic foraminifera shells. *Geochem Geophys Geosyst* 15(4):1452–1461.
10. Branson O, Kaczmarek K, Redfern SAT, Misra S (2015) The coordination and distribution of B in foraminiferal calcite. *Earth Planet Sci Lett* 416:67–72.
11. Spero HJ, et al. (2015) Timing and mechanism for intratest Mg/Ca variability in a living planktic foraminifer. *Earth Planet Sci Lett* 409:32–42.
12. Orme CA, et al. (2001) Formation of chiral morphologies through selective binding of amino acids to calcite surface steps. *Nature* 411(6839):775–779.
13. Falini G, Albeck S, Weiner S, Addadi L (1996) Control of aragonite or calcite polymorphism by mollusk shell macromolecules. *Science* 271(5245):67–69.
14. Wang D, Wallace AF, De Yoreo JJ, Dove PM (2009) Carboxylated molecules regulate magnesium content of amorphous calcium carbonates during calcification. *Proc Natl Acad Sci USA* 106(51):21511–21516.
15. Pouget EM, et al. (2009) The initial stages of template-controlled $CaCO_3$ formation revealed by cryo-TEM. *Science* 323(5920):1455–1458.
16. Smeets PJM, Cho KR, Kempen RGE, Sommerdijk NAJM, De Yoreo JJ (2015) Calcium carbonate nucleation driven by ion binding in a biomimetic matrix revealed by in situ electron microscopy. *Nat Mater* 14(4):394–399.
17. Pawlowski J, et al. (2003) The evolution of early Foraminifera. *Proc Natl Acad Sci USA* 100(20):11494–11498.
18. Spero HJ (1988) Ultrastructural examination of chamber morphogenesis and biomineralization in the planktonic foraminifer *Orbulina universa*. *Mar Biol* 99(1):9–20.
19. de Nooijer LJ, Spero HJ, Erez J, Bijma J, Reichart GJ (2014) Biomineralization in perforate foraminifera. *Earth Sci Rev* 135:1–11.
20. Robbins LL, Brew K (1990) Proteins from the organic matrix of core-top and fossil planktonic-foraminifera. *Geochim Cosmochim Acta* 54(8):2285–2292.
21. Stathopolos L, Tuross N (1994) Proteins and DNA from modern planktonic-foraminifera. *J Foraminiferal Res* 24(1):49–59.
22. Gotliv BA, Addadi L, Weiner S (2003) Mollusk shell acidic proteins: In search of individual functions. *ChemBioChem* 4(6):522–529.
23. Drake JL, et al. (2013) Proteomic analysis of skeletal organic matrix from the stony coral Stylophora pistillata. *Proc Natl Acad Sci USA* 110(10):3788–3793.
24. Addadi L, Weiner S (1985) Interactions between acidic proteins and crystals: Stereochemical requirements in biomineralization. *Proc Natl Acad Sci USA* 82(12):4110–4114.
25. Miller MK, Forbes RG (2014) *Atom-Probe Tomography* (Springer, New York).
26. Valley JW, et al. (2014) Hadean age for a post-magma-ocean zircon confirmed by atom-probe tomography. *Nat Geosci* 7(3):219–223.
27. Gordon LM, Joester D (2011) Nanoscale chemical tomography of buried organic-inorganic interfaces in the chiton tooth. *Nature* 469(7329):194–197.
28. Perea DE, et al. (2016) Atom probe tomographic mapping directly reveals the atomic distribution of phosphorus in resin embedded ferritin. *Sci Rep* 6:22321–22329.
29. Pérez-Huerta A, Laiginhas F, Reinhard DA, Prosa TJ, Martens RL (2016) Atom probe tomography (APT) of carbonate minerals. *Micron* 80:83–89.
30. Gagnon AC, Adkins JF, Erez J (2012) Seawater transport during coral biomineralization. *Earth Planet Sci Lett* 329-330:150–161.
31. Eggins S, Sadekov AY, de Deckker P (2004) Modulation and daily banding of Mg/Ca in *Orbulina universa* tests by symbiont photosynthesis and respiration: a complication for seawater thermometry? *Earth Planet Sci Lett* 225(3-4):411–419.
32. Branson O, et al. (2013) The coordination of Mg in foraminiferal calcite. *Earth Planet Sci Lett* 383:134–141.
33. Gault B, et al. (2006) Design of a femtosecond laser assisted tomographic atom probe. *Rev Sci Instrum* 77(4):043705.
34. Devaraj A, Colby R, Vurpillot F, Thevuthasan S (2014) Understanding atom probe tomography of oxide-supported metal nanoparticles by correlation with atomic-resolution electron microscopy and field evaporation simulation. *J Phys Chem Lett* 5(8):1361–1367.
35. Cuif J-P, Dauphin Y, Nehrke G, Nouet J, Perez-Huerta A (2012) Layered growth and crystallization in calcareous biominerals: Impact of structural and chemical evidence on two major concepts in invertebrate biomineralization studies. *Minerals* 2(1):11–39.
36. Lea DW, Mashiotta TA, Spero HJ (1999) Controls on magnesium and strontium uptake in planktonic foraminifera determined by live culturing. *Geochim Cosmochim Acta* 63(16):2369–2379.
37. Wit JC, de Nooijer LJ, Wolthers M, Reichart GJ (2013) A novel salinity proxy based on Na incorporation into foraminiferal calcite. *Biogeosciences* 10(10):6375–6387.
38. Giuffre AJ, Hamm LM, Han N, De Yoreo JJ, Dove PM (2013) Polysaccharide chemistry regulates kinetics of calcite nucleation through competition of interfacial energies. *Proc Natl Acad Sci USA* 110(23):9261–9266.
39. Hu Q, et al. (2012) The thermodynamics of calcite nucleation at organic interfaces: Classical vs. non-classical pathways. *Faraday Discuss* 159(0):509–523.
40. Walker JBA, Heywood BR, Mann S (1991) Oriented nucleation of $CaCO_3$ from metastable solutions under Langmuir monolayers. *J Mater Chem* 1(5):889–890.
41. Mann S, et al. (1993) Crystallization at inorganic-organic interfaces: Biominerals and biomimetic synthesis. *Science* 261(5126):1286–1292.
42. Lo Nostro P, Ninham BW (2012) Hofmeister phenomena: An update on ion specificity in biology. *Chem Rev* 112(4):2286–2322.
43. Hess B, van der Vegt NFA (2009) Cation specific binding with protein surface charges. *Proc Natl Acad Sci USA* 106(32):13296–13300.
44. Chaudhuri RG, Paria S (2009) Dynamic contact angles on PTFE surface by aqueous surfactant solution in the absence and presence of electrolytes. *J Colloid Interface Sci* 337(2):555–562.
45. Collins KD (2004) Ions from the Hofmeister series and osmolytes: Effects on proteins in solution and in the crystallization process. *Methods* 34(3):300–311.
46. Zavitsas AA (2001) Properties of water solutions of electrolytes and nonelectrolytes. *J Phys Chem B* 105:7805–7817.
47. Huber BT, Bijma J, Spero HJ (1996) Blue water scuba collection of planktic foraminifera. Methods and techniques of underwater research. *Proceedings of the American Academy of Underwater Sciences Scientific Diving Symposium, Smithsonian Institution, Washington DC*, eds Lang MA, Baldwin CC (American Academy of Underwater Sciences, Mobile, AL), pp 127–132.
48. Lea DW, Spero HJ (1992) Experimental determination of barium uptake in shells of the planktonic Methods and techniques of underwater research. *Geochim Cosmochim Acta* 56(7):2673–2680.
49. Miller MK, Russell KF, Thompson K, Alvis R, Larson DJ (2007) Review of atom probe FIB-based specimen preparation methods. *Microsc Microanal* 13(6):428–436.